Stable optical phase modulation with micromirrors

Caleb Knoernschild, Taehyun Kim, Peter Maunz, Stephen G. Crain, and Jungsang Kim*

Fitzpatrick Institute for Photonics, Electrical and Computer Engineering Department, Duke University, Durham, North Carolina 27708, USA

**jungsang@duke.edu*

Abstract: We measure the motional fluctuations of a micromechanical mirror using a Michelson interferometer, and demonstrate its interferometric stability. The position stability of the micromirror is dominated by the thermal mechanical noise of the structure. With this level of stability, we utilize the micromirror to realize an optical phase modulator by simply reflecting light off the mirror and modulating its position. The resonant frequency of the modulator can be tuned by applying a voltage between the mirror and an underlying electrode. Full modulation depth of $\pm\pi$ is achieved when the mirror resonantly excited with a sinusoidal voltage at an amplitude of 11V.

OCIS codes: (230.4685) Optical microelectromechanical devices; (230.4040) Mirrors; (120.5060) Phase modulation.

References and links

1. D. T. Neilson, R. Frahm, P. Kolodner, C. A. Bolle, R. Ryf, J. Kim, A. R. Papazian, C. J. Nuzman, A. Gasparyan, N. R. Basavanhally, V. A. Aksyuk, and J. V. Gates, "256 x 256 port optical cross-connect subsystem," J. Lightwave Technol. **22**, 1499–1509 (2004).
2. J. Kim, C. J. Nuzman, B. Kumar, D. F. Lieuwen, J. S. Kraus, A. Weiss, C. P. Lichtenwalner, A. R. Papazian, R. E. Frahm, N. R. Basavanhally, D. A. Ramsey, V. A. Aksyuk, F. Pardo, M. E. Simon, V. Lifton, H. B. Chan, M. Haueis, A. Gasparyan, H. R. Shea, S. Arney, C. A. Bolle, P. R. Kolodner, R. Ryf, D. T. Neilson, and J. V. Gates, "1100 x 1100 port MEMS-based optical crossconnect with 4-dB maximum loss," IEEE Photon. Technol. Lett. **15**, 1537–1539 (2003).
3. R. A. Conant, P. M. Hagelin, U. Krishnamoorthy, M. Hart, O. Solgaard, K. Y. Lau, and R. S. Muller, "A raster-scanning full-motion video display using polysilicon micromachined mirrors," Sens. Actuators A **83**, 291–296 (2000).
4. K. Castelino, V. Milanovic, and D. McCormick, "MEMS-based high-speed low-power vector display," International Conference on Optical MEMS and Their Applications IEEE/LEOS (IEEE, 2005), pp. 127 –128.
5. D. L. Moehring, M. J. Madsen, K. C. Younge, R. N. Kohn, Jr., P. Maunz, L.-M. Duan, C. Monroe, and B. B. Blinov, "Quantum networking with photons and trapped atoms," J. Opt. Soc. Am. B **24**, 300–315 (2007).
6. L. Luo, D. Hayes, T. Manning, D. Matsukevich, P. Maunz, S. Olmschenk, J. Sterk, and C. Monroe, "Protocols and techniques for a scalable atom-photon quantum network," Fortschr. Phys. **57**, 1133–1152 (2009).
7. C. Knoernschild, C. Kim, F. P. Lu, and J. Kim, "Multiplexed broadband beam steering system utilizing high speed MEMS mirrors," Opt. Express **17**, 7233–7244 (2009).
8. C. Knoernschild, X. L. Zhang, L. Isenhower, A. T. Gill, F. P. Lu, M. Saffman, and J. Kim, "Independent individual addressing of multiple neutral atom qubits with a micromirror-based beam steering system," Appl. Phys. Lett. **97**, 134101 (2010).
9. M. Gottlieb, C. L. M. Ireland, and J. M. Ley, *Electro-Optic and Acousto-Optic Scanning and Deflection* (M. Dekker, 1983).
10. F. Schmidt-Kaler, H. Häffner, S. Gulde, M. Riebe, G. Lancaster, T. Deuschle, C. Becher, W. Hänsel, J. Eschner, C. Roos, and R. Blatt, "How to realize a universal quantum gate with trapped ions," Appl. Phys. B **77**, 789–796 (2003).

#157571 - $15.00 USD Received 9 Nov 2011; revised 20 Jan 2012; accepted 22 Jan 2012; published 27 Jan 2012

11. S. Kim, R. R. Mcleod, M. Saffman, and K. H. Wagner, "Doppler-free, multiwavelength acousto-optic deflector for two-photon addressing arrays of Rb atoms in a quantum information processor," Appl. Opt. **47**, 1816–1831 (2008).
12. S. X. Wang, J. Labaziewicz, Y. Ge, R. Shewmon, and I. L. Chuang, "Demonstration of a quantum logic gate in a cryogenic surface-electrode ion trap," Phys. Rev. A **81**, 062332 (2010).
13. C. Kim, C. Knoernschild, B. Liu, and J. Kim, "Design and characterization of MEMS micromirrors for ion-trap quantum computation," IEEE J. Sel. Top. Quantum Electron. **13**, 322–329 (2007).
14. M. Andrews, I. Harris, and G. Turner, "A comparison of squeeze-film theory with measurements on a microstructure," Sens. Actuators A **36**, 79–87 (1993).
15. C. Knoernschild, C. Kim, B. Liu, F. P. Lu, and J. Kim, "MEMS-based optical beam steering system for quantum information processing in two-dimensional atomic systems," Opt. Lett. **33**, 273–275 (2008).
16. B. E. A. Saleh and M. C. Teich, *Fundamentals of Photonics* (Wiley-Interscience, 2007).
17. Z. Djuric, "Mechanisms of noise sources in microelectromechanical systems," Microelectron. Reliab. **40**, 919–932 (2000).
18. J. E. Debs, N. P. Robins, A. Lance, M. B. Kruger, and J. D. Close, "Piezo-locking a diode laser with saturated absorption spectroscopy," Appl. Opt. **47**, 5163–5166 (2008).

1. Introduction

Micromirrors fabricated using micro-electromechanical systems (MEMS) technology are well suited to steer a potentially large number of laser beams. MEMS systems are used in all-optical switching [1, 2], scanning projection displays [3, 4], and optical addressing of quantum information processing systems [5–8]. Compared to traditional beam steering techniques such as acousto-optic (AO) and electro-optic (EO) deflectors [9–11], MEMS-based approaches typically consume much less actuation energy and device volume per beam. These advantages make scalable systems capable of simultaneously steering a large number of beams possible. In many applications in quantum information processing with atoms, the optical phases of the multiple beams addressing the atomic qubits have to be maintained [12].

In this paper, we present a characterization of the pointing and phase stability of MEMS mirrors. Using a Michelson interferometer, we demonstrate interferometric stability of carefully designed micromirrors. These micromirrors are shown to have motional stability down to thermal noise levels. Taking advantage of the interferometric stability, scalability, and low actuation requirements of MEMS mirrors, we introduce a method of MEMS-based optical phase modulation. Resonant vibrations of the MEMS mirrors, which are frequency tunable with bias voltage, are shown to enable controllable optical phase modulation at radio frequencies (RF). With this modulation scheme, phase modulation on multiple laser systems can be performed in a single, high optical density device.

2. MEMS mirror design

We consider a micromirror consisting of a circular polysilicon mirror plate tethered to anchors with two torsional springs (Fig. 1(a)) [13]. The MEMS structure is fabricated using Sandia's SUMMiT V MEMS foundry process, where alternating layers of polysilicon (structural and routing layers) and silicon dioxide (SiO_2: sacrificial layers) are used to form the devices. At the end of the fabrication process, the SiO_2 is selectively removed to enable free motion of the polysilicon structural layers. The released mirror is electrostatically actuated by applying a voltage between the grounded mirror plate and the underlying electrodes. The mirror structure features several mechanical modes of vibration with the lowest resonant frequencies corresponding to the tilting and sagging modes. The behavior of these modes can be captured using

#157571 - $15.00 USD Received 9 Nov 2011; revised 20 Jan 2012; accepted 22 Jan 2012; published 27 Jan 2012

a damped harmonic oscillator model:

$$I\ddot{\theta} + D_\theta \dot{\theta} + 2\kappa\theta = \frac{1}{2}\frac{\partial C(\theta,z)}{\partial \theta}V^2 + F_\theta, \quad (1)$$

$$M\ddot{z} + D_z \dot{z} + 2Kz = \frac{1}{2}\frac{\partial C(\theta,z)}{\partial z}V^2 + F_z, \quad (2)$$

where θ and z are the variables describing the tilt angle and vertical sag of the mirror plate, respectively. Variables I (M), D_θ (D_z), κ (K), $C(\theta,z)$, V and $F_{\theta(z)}$ denote the rotational inertia (mass) of the mirror plate, damping coefficient for the tilting (sagging) mode, torsional stiffness (spring constant) of the torsional springs, capacitance between the mirror plate and the underlying actuation electrode, applied voltage between the electrode and the mirror plate, and other driving torque (force) for the tilting (sagging) mode, respectively. The mirror features a tilting (sagging) resonance in the θ direction at $\omega_\theta = \sqrt{2\kappa/I}$ (z direction at $\omega_z = \sqrt{2K/M}$). Modes with higher resonant frequencies exist that involve higher-order distortion of the mirror plate. The dominant damping mechanism for the mirror motion is squeeze film damping by the air between the mirror plate and the substrate [14]. For optimal beam steering performance, the mirror is designed to feature near critical damping for the tilt motion at atmospheric pressures [13, 15]. The damping can be reduced by either placing the mirror in vacuum, or by modifying the device design to provide smaller mirror radius and larger gap between the mirror and the substrate.

The spectral response of the primary tilting mode to a driving torque in the absence of applied voltage ($V = 0$) can be calculated by solving Eq. (1) in Fourier domain:

$$|\tilde{\theta}(\omega)|^2 = \frac{|\tilde{F}_\theta(\omega)|^2}{(2\kappa)^2}\frac{1}{(1-\omega^2/\omega_\theta^2)^2 + \omega^2/(Q^2\omega_\theta^2)}, \quad (3)$$

where $Q = \sqrt{2\kappa I}/D_\theta$ is the quality factor of the tilting mode, and $\tilde{\theta}(\omega)$ and $\tilde{F}_\theta(\omega)$ are the Fourier transform of the tilt angle and the angular driving torque, respectively.

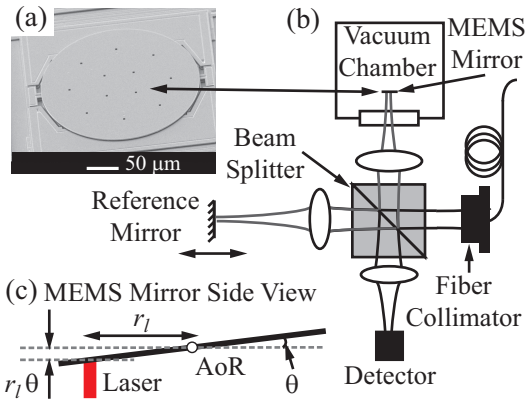

Fig. 1. Schematic of the measurement setup. (a) Scanning electron micrograph of a MEMS mirror. (b) MEMS mirror stability measurement setup using a Michelson interferometer. (c) Shifting the reflection point on the MEMS mirror for sensitivity in the tilting mode.

#157571 - $15.00 USD Received 9 Nov 2011; revised 20 Jan 2012; accepted 22 Jan 2012; published 27 Jan 2012

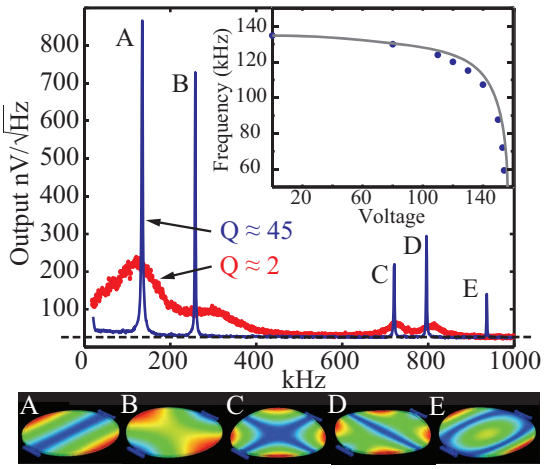

Fig. 2. Interferometer output representing the position noise spectrum of a micromirror at a pressure of 5 Torr ($Q \approx 45$) and 760 Torr ($Q \approx 2$) with 0V bias voltage. The dotted line shows shot noise level corresponding to laser intensity fluctuations. Simulations of the mode shapes corresponding to the five peaks (A – E) are shown by a color plot of maximum displacement. The inset shows tuning of tiling mode resonant frequency as a function of bias voltage. Dots indicate measured data while the solid line shows the theoretical prediction.

3. Stability measurement

We measured the pointing stability of this MEMS mirror in a Michelson interferometer, as shown in Fig. 1(b). A single mode, $\lambda = 780$ nm wavelength laser diode is directed to a 50/50 beam splitter. Half of the light is sent toward the MEMS device in the sample arm of the interferometer and the other half onto a standard mirror in the reference arm. The light in the sample arm is focused by a 50 mm focal length lens to a beam waist of 15 μm at the MEMS mirror. The MEMS mirror has a radius of $R = 130$ μm and resonant frequency of $\omega_\theta/2\pi = 135$ kHz for the tiling mode ($\omega_z/2\pi = 258$ kHz for sagging mode). It is housed inside a vacuum chamber to control the damping. Light in the reference arm of the interferometer travels through a second 50 mm focal length lens before reflecting off the standard flat mirror. The standard mirror is mounted on a kinematic mount with a piezoelectric actuator to tune the optical path length difference of the interferometer. Light from the two arms recombines on the beam splitter before a final lens focuses it onto a photodetector. The photocurrent measured by the photodetector, assuming no losses, follows the standard interference equation and is given by $I_{det} = I_{ph}[1+\cos(2\pi d_{opt}/\lambda + \phi_i)]/2$, where I_{ph} is the photocurrent proportional to the optical power used in the interferometer, d_{opt} is the optical path length introduced by the micromirror motion, and ϕ_i is the bias point of the interferometer determined by the position of the standard mirror [16]. The interferometer is actively stabilized at $\phi_i = \pi/2$ to maximize sensitivity.

The sagging mode of the mirror changes the path length in the sample arm by slightly shifting the reflection plane along the direction of propagation. The tilting motion induces a tilt in the sample arm beam path, and does not lead to an optical path length change in the interferometer. A path length change using the tilting mode is realized by aligning the beam to reflect off the mirror a distance $r_l \approx 0.75R$ away from the axis of rotation (Fig. 1(c)), leading to $d_{opt} = 2r_l\theta$.

Figure 2 shows the noise spectrum of the interferometer output, corresponding to the phase noise arising from the motion of the micromirror. The two curves correspond to operating the mirror in a background pressure of ~ 5 and 760 Torr with a corresponding quality factor $Q \approx 45$

#157571 - $15.00 USD Received 9 Nov 2011; revised 20 Jan 2012; accepted 22 Jan 2012; published 27 Jan 2012

and 2 for the primary tilting mode, respectively. The photocurrent from the detector is converted to a voltage signal using a transimpedance amplifier with tranimpedance gain of R_f = 2 kΩ. The detected photocurrent of $I_{ph} = 0.6$mA from 1.5mW of optical power received at the detector corresponds to an optical shot noise level of $\sqrt{2qI_{ph}}R_f \approx 28\text{nV}/\sqrt{\text{Hz}}$, where q is the absolute value of the electron charge (dashed line). This shot noise value describes the fundamental sensitivity of the interferometer's ability to detect a phase shift with a noise level of $\sim 5\times10^{-8}$ rad/$\sqrt{\text{Hz}}$. The source laser diode used in our experiment has inherently low intensity noise, featuring shot noise level above 400kHz, and only a modest increase (by a factor of two) for frequencies down to 30 kHz without any additional stabilization technique.

Fluctuations in micromirror position is primarily driven by thermal mechanical noise force [17] with (frequency-independent) power spectral density of $|\tilde{F}_{\theta(z)}(\omega)|^2 = 4k_BTD_{\theta(z)}$. In this expression, k_B is the Boltzmann constant and T is the operating temperature of the mirror. The angle (position) of the mirror responds to this driving force according to Eq. (1) and (2), and angular tilt results in the change in mirror position at the point of reflection (Fig. 1(c)). The peaks in Fig. 2 show the resulting position noise corresponding to five lowest normal modes of the micromirror (labeled A – E, the maximum displacement of the mode shown at the bottom). When integrated over the full spectrum, thermal noise from each mechanical mode will correspond to an equivalent energy of $k_BT/2$ due to equipartition theorem. From the torsional stiffness of $2\kappa = 1.7\times10^{-6}$Nm (spring constant of $2K = 1.4\times10^{3}$N/m) extracted from the resonant frequency, the integrated RMS tilt angle (position) noise from main tilting mode is $\sim 5\times10^{-8}$rad ($\sim$ 1.7pm for sagging mode). This value can also be obtained by integrating the power spectral density given in Eq. (3) over the entire frequency range. The peak of the noise power spectral density is related to the integrated noise power by a factor of $\sim\sqrt{4Q/\omega_\theta}$ according to Eq. (3). The peak tilt angle noise $\delta\theta_{max}$ is converted into the interferometer phase noise of $\delta\phi_{max} = 4\pi r_l\delta\theta_{max}/\lambda$, which is then converted to the voltage noise at the output of the transimpedance amplifier by the relationship $\delta V_{max} = I_{ph}\delta\phi_{max}R_f/2$. For the main tilting mode, the expected peak height arising from the mechanical thermal noise is 690 nV/$\sqrt{\text{Hz}}$ and 145 nV/$\sqrt{\text{Hz}}$ for the $Q = 45$ and $Q = 2$ case, respectively, which is consistent with the measured values within a factor of 2. From this analysis, we conclude that the total intrinsic noise from the micromirror contributing to the RMS phase noise of the optical field is less than 10^{-4} rad.

When a DC bias voltage is applied between the mirror and underlying electrode, the resonance frequency of the mechanical oscillator shifts to a lower value. The nonlinearity inherent in capacitive actuation (right hand side of Eqs. (1) and (2) produces greater electrostatic forces for a given voltage at higher angles of tilt. The inset in Fig. 2 illustrates this effect known as electrostatic softening for the tilting mode. Data points are plotted against the theoretical behavior which is calculated based on measured values of the mirror's mechanical constants and simulated capacitance values. This mechanism can be used to tune the resonant frequency of a given mechanical oscillator.

4. Phase modulation

The demonstrated stability of the mirror suggests that the resonant modes of the micromirrors can be utilized to modulate the phase of an optical field at RF with low additional phase noise. The depth of modulation for a micromirror driven at mechanical resonance is amplified by the quality factor Q, enabling significant modulation with only modest driving voltages. Furthermore, the resonant frequency of the micromirror can be tuned using electrostatic softening. We characterized the optical phase modulation properties with the Michelson interferometer (Fig. 1(b)) using the sagging mode at 258kHz and reflecting the laser beam at the center of the micromirror. When the optical path length difference is modulated by $(\beta\lambda/2\pi)\sin\omega t$, the

#157571 - $15.00 USD Received 9 Nov 2011; revised 20 Jan 2012; accepted 22 Jan 2012; published 27 Jan 2012

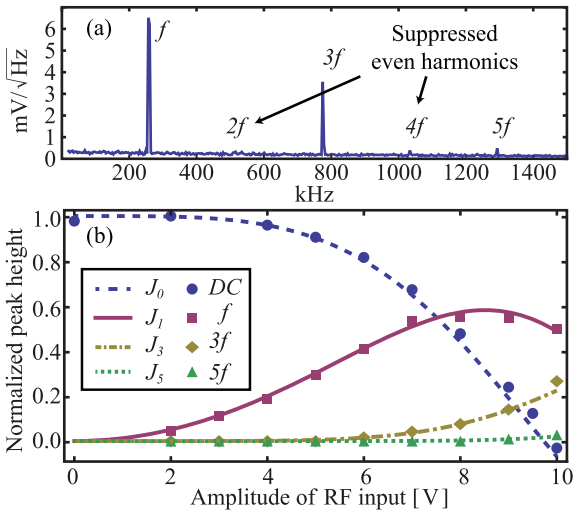

Fig. 3. (a) Spectrum of interferometer output for a given modulation amplitude of a sagging mode at f =258 kHz. (b) Normalized spectrum peak heights as a function of RF voltage amplitude. Bessel functions of different orders $J_n(s \cdot v_d^2)$ are plotted using a single fitting parameter $s = 0.025/V^2$ (lines), while the measured DC values (circles) and peak heights are shown with squares (f), diamonds ($3f$), and triangles ($5f$).

detected current I_{det} is given by

$$\begin{aligned} I_{det} &\propto 1+\cos(\phi_i+\beta\sin\omega t) = 1+J_0(\beta)\cos\phi_i \\ &\quad +2\{J_2(\beta)\cos 2\omega t + J_4(\beta)\cos 4\omega t+\cdots\}\cos\phi_i \\ &\quad -2\{J_1(\beta)\sin\omega t + J_3(\beta)\sin 3\omega t+\cdots\}\sin\phi_i. \end{aligned} \tag{4}$$

In the experiment, we set $\phi_i = \pi/2$ to suppress all even order modulation sidebands. Due to quadratic dependence on the applied voltage shown in Eq. (2), we use a RF voltage at frequency $f/2$ to induce a phase modulation at frequency f. Depth of the optical path length modulation is proportional to the square of the amplitude of the driving RF voltage v_d, so we let $\beta \equiv s \cdot v_d^2$ to define the proportionality constant s. Figure 3(a) shows a spectrum of the interferometer output when the micromirror is driven with RF voltage amplitude of $v_d = 10$V. The even order modulation sidebands are suppressed, and the relative peak heights of the odd order modulation sidebands can be determined. By fitting the peak heights of first order modulation sideband to $A \cdot J_1(s \cdot v_d^2)$ as a function of v_d, we obtained $s = 0.025 \pm 0.0005/V^2$.

We plot the peak heights of each odd order modulation sideband as a function of the RF voltage amplitude in Fig. 3(b). The DC components corresponding to $J_0(s \cdot v_d^2)$ are measured by scanning ϕ_i from 0 to $\pi/2$ for each RF amplitude, and fit using the s value obtained from first order modulation sidebands. The amplitude of J_0 values have to be normalized since the DC and AC current are measured using different transimpedance gain in our circuit. The data fit well to Bessel functions with a single scaling parameter s up to fifth order. A DC voltage of 135V is necessary to induce a phase shift of π for the 780 nm laser for this mirror, but a smaller RF voltage amplitude of $v_d \approx 11$ V is sufficient to generate phase oscillation between $\pm\pi$ when a mechanical resonance is utilized. The reduction in driving voltage is consistent with the quality factor $Q_s \sim 300$ of the sagging mode under the operating pressure. The contribution of mechanical thermal noise of the mirrors on the RMS phase noise of the modulator is inde-

#157571 - $15.00 USD Received 9 Nov 2011; revised 20 Jan 2012; accepted 22 Jan 2012; published 27 Jan 2012

pendent of the quality factor of the mechanical resonance used, and was estimated to be less than 10^{-4} rad in Section 3.

Phase modulation based on reflection off a micromirror works over a broad wavelength range, and is insensitive to polarization, power of the incoming light and potential thermal drifts from driving RF power. Using micromirrors with higher resonant frequencies, higher modulation frequencies can be achieved than by using macroscopic mirrors [18]. A large array of such micromirror-based phase modulators can be fabricated in a single chip in the case where a scalable solution is desired.

5. Summary

In this work, we showed that micromirrors can be used to construct beam steering devices with interferometric phase stability. This stability was shown to be limited by thermal noise associated with the mechanical structure of the mirror. The resonant modes excited by the thermal noise of the MEMS device were identified and frequency controlled with a DC bias voltage. Leveraging the stability, tunability, scalability, and low actuation requirements associated with MEMS mirrors, we propose a MEMS-based optical phase modulating system and demonstrate $\pm\pi$ phase oscillations at 258 kHz driven by an RF amplitude of 11 V. Micromirrors designed for higher modulation frequencies could easily provide MHz phase oscillations. This MEMS-based phase modulation system could enable phase control of multiple laser systems across a range of wavelengths using only a single device.

Acknowledgments

The authors would like to thank Felix P. Lu at Applied Quantum Technologies in Durham, North Carolina for help with the micromirrors. This work was supported by ARO, office of the Director of National Intelligence, and Intelligence Advanced Research Projects Activity.

#157571 - $15.00 USD Received 9 Nov 2011; revised 20 Jan 2012; accepted 22 Jan 2012; published 27 Jan 2012